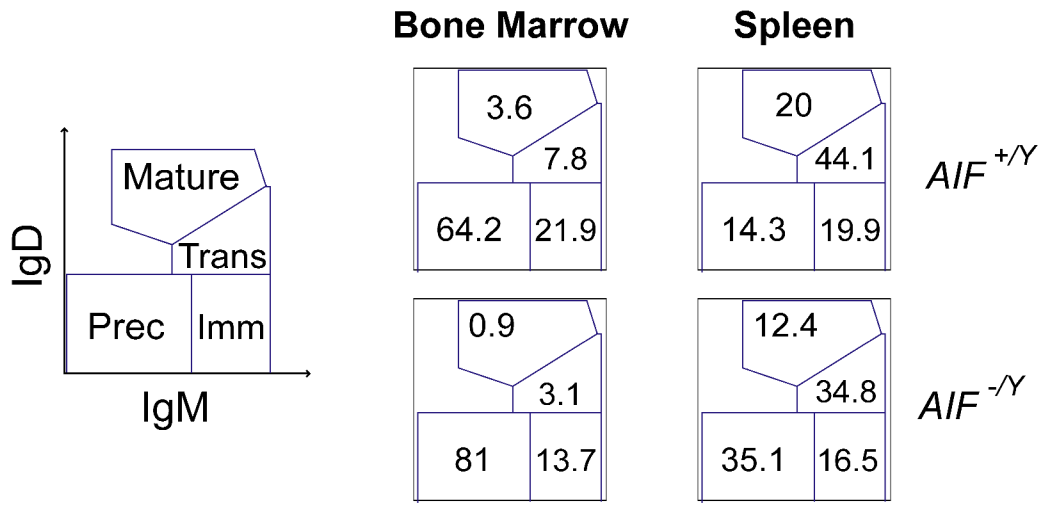

Supplementary Table 1. *AIF* $^{-/Y}$ mice presented increased frequencies of precursor B-cells in BM and spleen. *Left,* Gating strategy. *Rigth,* Representative results of a IgD/IgM staining per formed in B220-expressing BM and spleen cells from 21-day-old *AIF* $^{+/Y}$ and *AIF* $^{-/Y}$ animals. The percentages of mature (IgM+IgD+), transitional (Trans, IgM+IgDint), immature (Imm, IgM+IgD-), and precursor (Prec, IgM-IgD-) B-cells are shown. These data are depicted in Figure 1g.

Pathways	Total	Expected	Hits	Raw p	Holm p	FDR	Impact
Aminoacyl-tRNA biosynthesis	69	0.88	11	3.98E-11	3.26E-09	3.26E-09	0.00
Arginine and proline metabolism	44	0.56	5	1.45E-04	1.18E-02	5.96E-03	**0.32**
Valine, leucine and isoleucine biosynthesis	11	0.14	3	2.67E-04	2.14E-02	7.30E-03	**1.00**
Alanine, aspartate and glutamate metabolism	24	0.30	3	2.95E-03	2.33E-01	6.05E-02	**0.15**
Nitrogen metabolism	9	0.11	2	5.21E-03	4.06E-01	8.54E-02	0.00
Valine, leucine and isoleucine degrada-tion	38	0.48	3	1.10E-02	8.47E-01	1.50E-01	0.00
Glutathione metabolism	26	0.33	2	4.14E-02	1.00E+00	4.24E-01	0.01
Galactose metabolism	26	0.33	2	4.14E-02	1.00E+00	4.24E-01	**0.04**
Glycine, serine and threonine metabolism	31	0.39	2	5.70E-02	1.00E+00	5.08E-01	**0.27**
D-Glutamine and D-glutamate metabolism	5	0.06	1	6.20E-02	1.00E+00	5.08E-01	0.00
Cyanoamino acid metabolism	6	0.08	1	7.40E-02	1.00E+00	5.51E-01	0.00
Methane metabolism	9	0.11	1	1.09E-01	1.00E+00	7.45E-01	0.00
Selenoamino acid metabolism	15	0.19	1	1.75E-01	1.00E+00	1.00E+00	0.00
Pantothenate and CoA biosynthesis	15	0.19	1	1.75E-01	1.00E+00	1.00E+00	0.00
Glyoxylate and dicarboxylate metabolism	18	0.23	1	2.07E-01	1.00E+00	1.00E+00	0.00
Starch and sucrose metabolism	19	0.24	1	2.17E-01	1.00E+00	1.00E+00	**0.04**
Citrate cycle (TCA cycle)	20	0.25	1	2.27E-01	1.00E+00	1.00E+00	**0.05**
Fructose and mannose metabolism	21	0.27	1	2.37E-01	1.00E+00	1.00E+00	**0.13**
Pyruvate metabolism	23	0.29	1	2.56E-01	1.00E+00	1.00E+00	0.00
Porphyrin and chlorophyll metabolism	27	0.34	1	2.94E-01	1.00E+00	1.00E+00	0.00
Cysteine and methionine metabolism	27	0.34	1	2.94E-01	1.00E+00	1.00E+00	**0.09**
Glycerophospholipid metabolism	30	0.38	1	3.21E-01	1.00E+00	1.00E+00	0.00
Pyrimidine metabolism	41	0.52	1	4.12E-01	1.00E+00	1.00E+00	0.00
Tyrosine metabolism	44	0.56	1	4.35E-01	1.00E+00	1.00E+00	0.03
Primary bile acid biosynthesis	46	0.58	1	4.50E-01	1.00E+00	1.00E+00	0.03
Purine metabolism	68	0.86	1	5.90E-01	1.00E+00	1.00E+00	0.00

Supplementary Table 2. AIF loss-mediated OXPHOS dysfunction induced metabolic adjustments in BM cells. Detailed results obtained in broad metabolic assessments of BM cells from 21-day-old *AIF* $^{+/Y}$ and *AIF* $^{-/Y}$ mice analyzed using the Metabolomics pathway (MetPA) software (freely available at http://metpa.metabolomics.ca). The data are expressed as the results recorded in the *AIF* $^{-/Y}$ cells compared to *AIF* $^{+/Y}$ cells. Statistical p values are as follows: (i) Total is the total number of compounds in a pathway; (ii) Hits represent the matched number from user uploaded data; (iii) Raw p is the original p-value calculated from the enrichment analysis; (iv) Holm p represents the p-value adjusted using the Holm-Bonferroni method; (v) FDR is the p-value adjusted using the False Discovery Rate; and (vi) Impact depicts the pathway impact value calculated based on a pathway topology analysis. In terms of impact, the metabolic pathways altered by the loss of AIF are shown in bold.

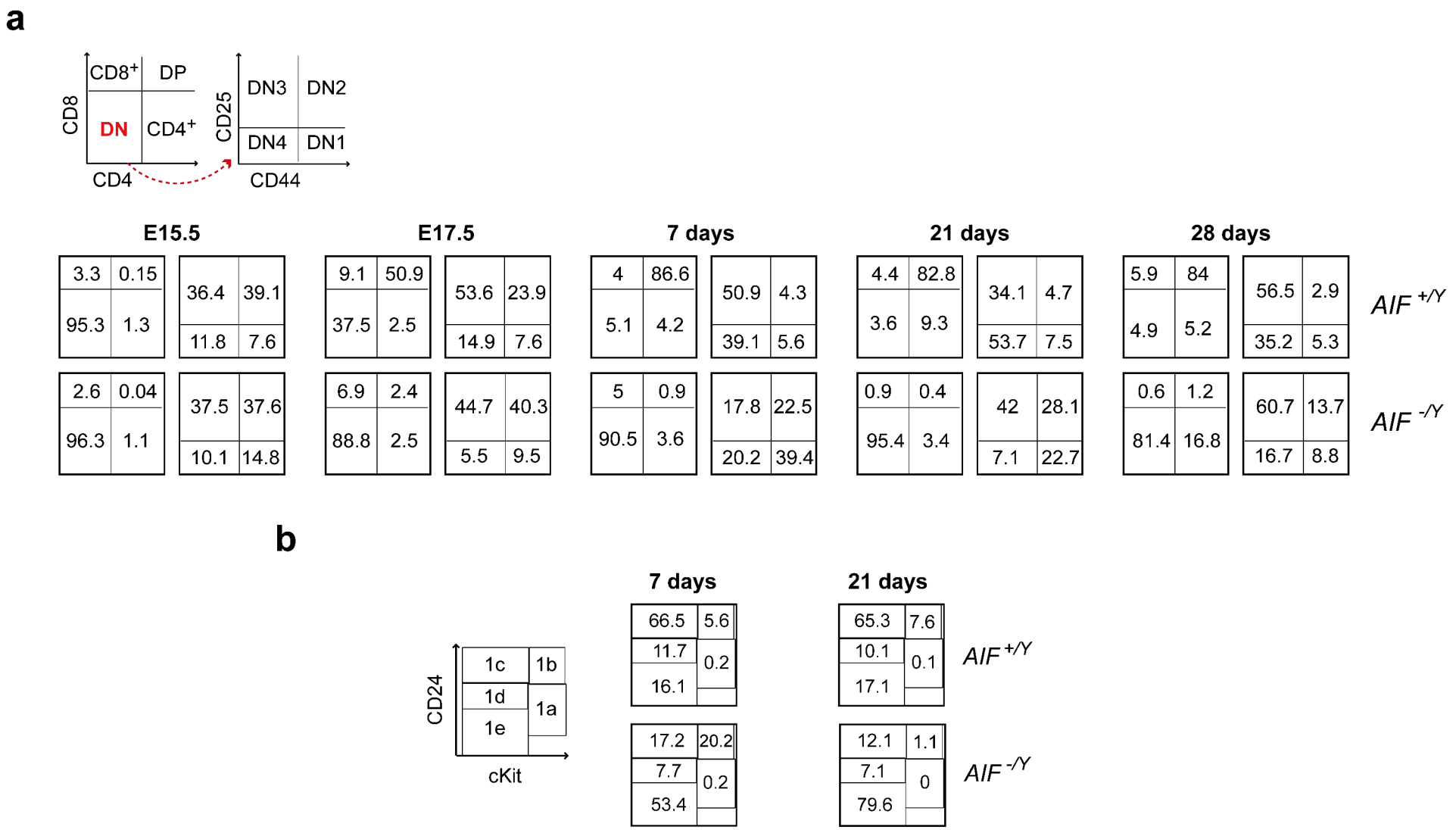

Supplementary Table 3. AIF loss led to a blockade of thymopoiesis at a DN immature state with DN1 accumulation and delayed DN2/DN3 and DN3/DN4 transitions. DN1 prothymocytes are characterized by low levels of the DN1c subset, a progressive exhaustion of the canonical T pro genitors DN1a/DN1b, and the accumulation of DN1e cells. (**a**) The staining with CD4/CD8 and CD44/CD25 antibodies were performed in thymocytes from E15.5 and E17.5 embryos and 7, 21, and 28-day-old *AIF* $^{+/Y}$ and *AIF* $^{-/Y}$ animals. The gating strategy and a representative percentage of cells in the flow cytometry panels are indicated. (**b**) The frequencies of DN1 subsets were recorded on thymocytes from 7 and 21-day-old *AIF* $^{+/Y}$ and *AIF* $^{-/Y}$ animals. Typical percentages of DN1a (cKit+CD24low), DN1b (cKit+CD24+), DN1c (cKit-CD24+), DN1d (cKit-CD24 low), and DN1e (cKit-CD24-) cells are shown. These data are depicted as histograms in Figures 5a and b.

a

	CD	CD NAC
WT	17,467	13,584
AIF KO	6,547	4,187
	HFD	**HFD NAC**
WT	13,212	17,815
AIF KO	8,001	23,798

b

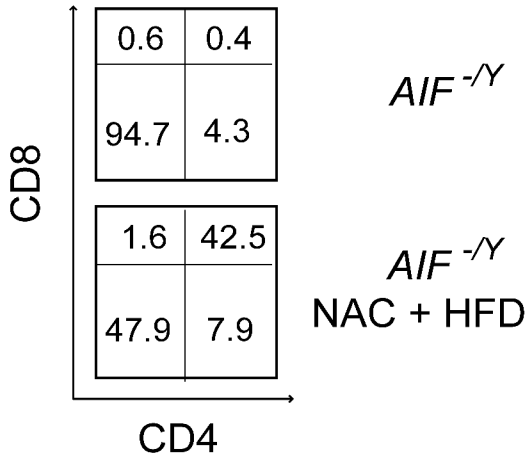

Supplementary Table 4. High fat diet and antioxidant combined treatments restored ATP levels and thymopoiesis in *AIF*$^{-/Y}$ mice. (**a**) Representative ATP levels recorded in WT and AIF KO thymocytes from 21-day-old newborns from dams fed with control diet (CD) or high-fat diet (HFD) and supplied or not with NAC in drinking water (n = 9 animals per group). (**b**) Typical percentages of a CD4/CD8 labeling measured in *AIF*$^{-/Y}$ thymocytes purified from mice animals fed with a control diet (*AIF*$^{-/Y}$) or with a HFD supplied with NAC (*AIF*$^{-/Y}$ NAC + HFD). These data are represented in the histograms included in the Figures 7e and f.

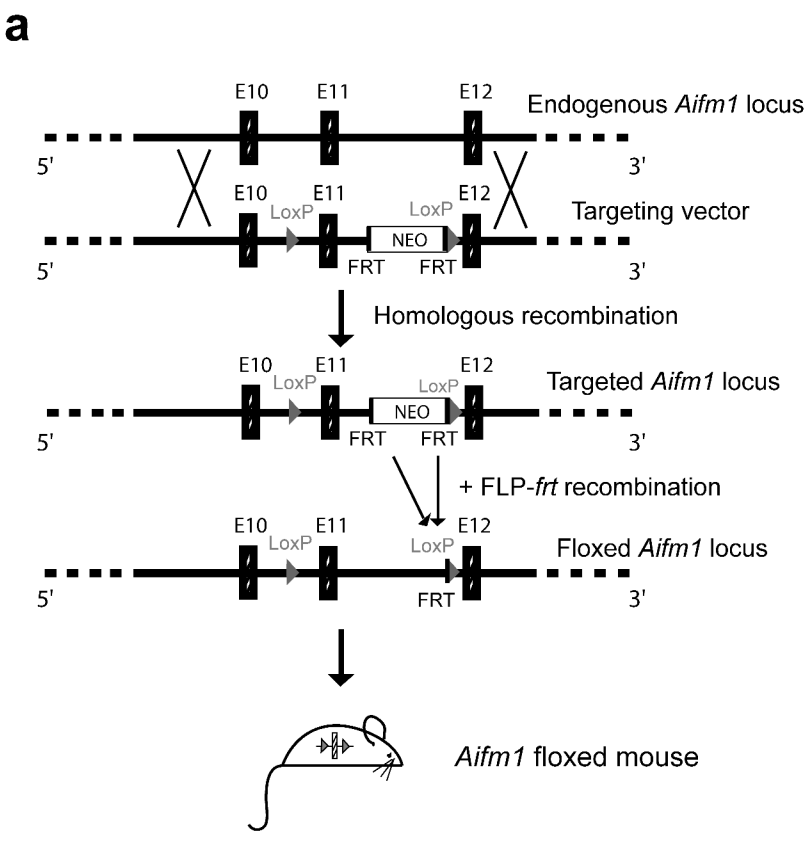

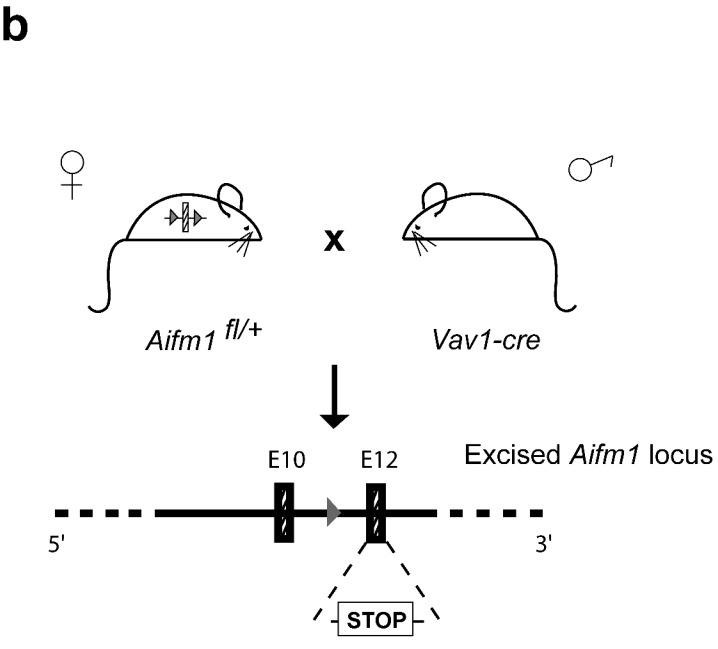

c

Aifm1$^{fl/+}$ x *Vav1-cre*:

(Among males)	*AIF* $^{+/Y}$	*AIF* $^{-/Y}$
Expected	563 (50%)	563 (50%)
Observed	592 (53%)	534 (47%)

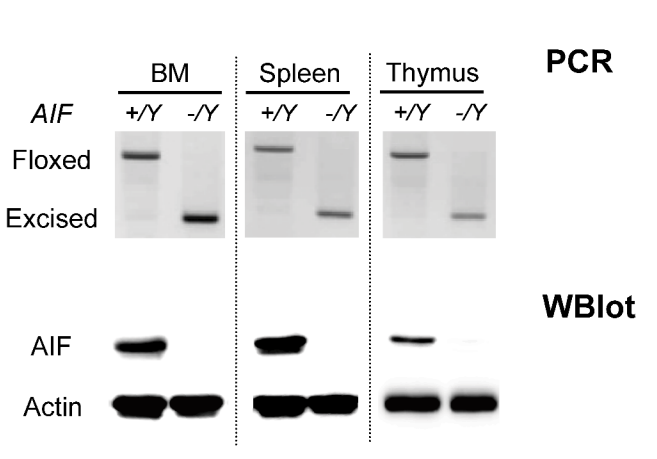

Supplementary Figure 1. Generation of a hematopoietic cell-specific *AIF* $^{-/Y}$ mouse strain. (**a**) Schematic representation of the wild-type *Aifm1* allele (top), targeting vector (middle), the targeted *Aifm1* locus, and the resulting floxed *Aifm1* locus. The targeting vector was generated by classical recombination. Briefly, exon 11 of *Aifm1* was flanked by LoxP sequences in direct orientation along with a NEO cassette used for selection. Then, Sv129 ES cells were electroporated with this vector, transfected with a plasmid containing FLP recombinase to eliminate the NEO cassette and, after se lecting positive clones, injected into C57Bl/6J blastocysts to obtain the chimeric mice. (**b**) After at le ast fifteen backcrosses to the C57BL/6J background, heterozygous *Aifm1*-floxed females (*Aifm1* $^{fl/+}$) were crossed to C57BL/6J Vav1-cre males. This crossing induced the excision of exon 11 in *Aifm1* that resulted in a frameshift mutation and the creation of a stop codon in exon 12. (**c**) Generation of male offspring from crosses of *Aifm1* $^{fl/+}$ females with C57BL/6J Vav1-cre males (Observed) compa red with the theoretical Mendelian distribution (Expected). (**d**) Genomic PCR assessment of exon 11 of the *Aifm1* locus in BM cells, splenocytes, and thymocytes from *AIF* $^{+/Y}$ and *AIF* $^{-/Y}$ neonate mice. AIF immunoblotting confirmed total AIF ablation.

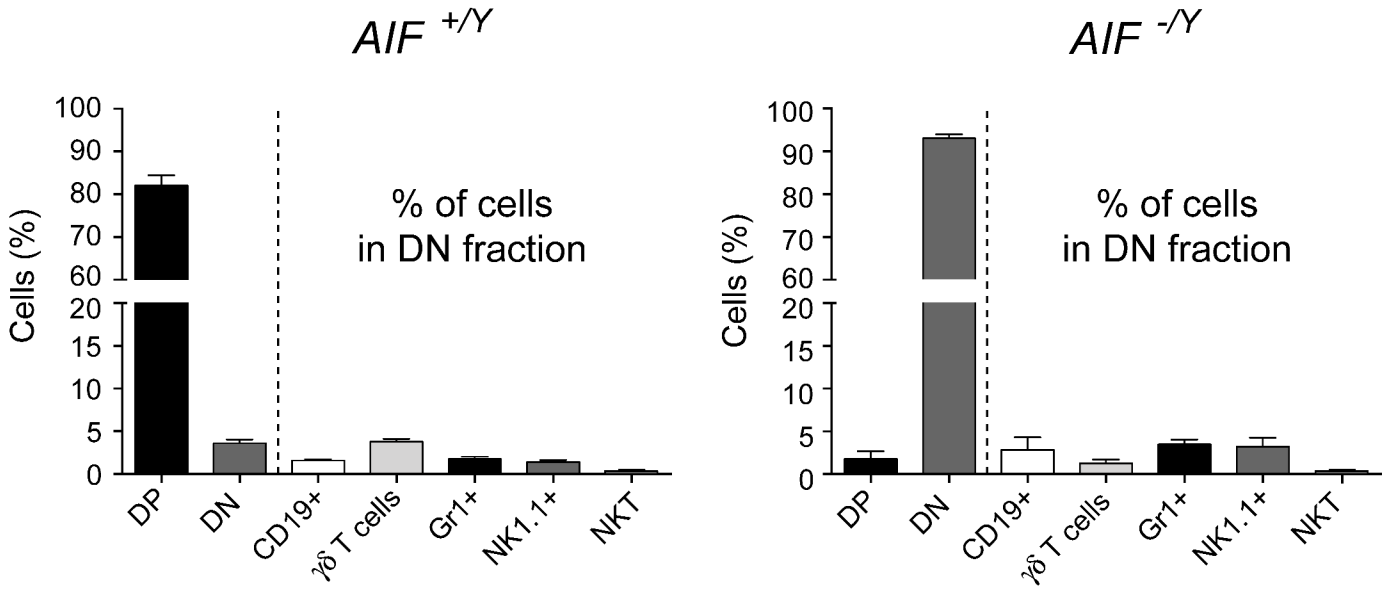

Supplementary Figure 2. Percentage of B cells, myeloid cells, γδ T cells, NK cells, NK T cells that are present in the DN thymocyte fraction purified from *AIF*$^{+/Y}$ *and AIF* $^{-/Y}$ animals. The percentages of DP and DN cells were assessed in 21-day-old *AIF*$^{+/Y}$ and *AIF* $^{-/Y}$ mice by a double CD4/CD8 labeling. Then, in the DN fractions, the percentages of B cells (CD19+), γδ T cells (γδ+), Myeloid cells (Gr1+), NK cells (NK1.1+) and NKT cells (NK1.1+ CD3+) were measured and expressed as a histogram (n = 5 animals per group). Statistical signifi cance was calculated by Mann Whitney test. Bars represent mean ± SEM.

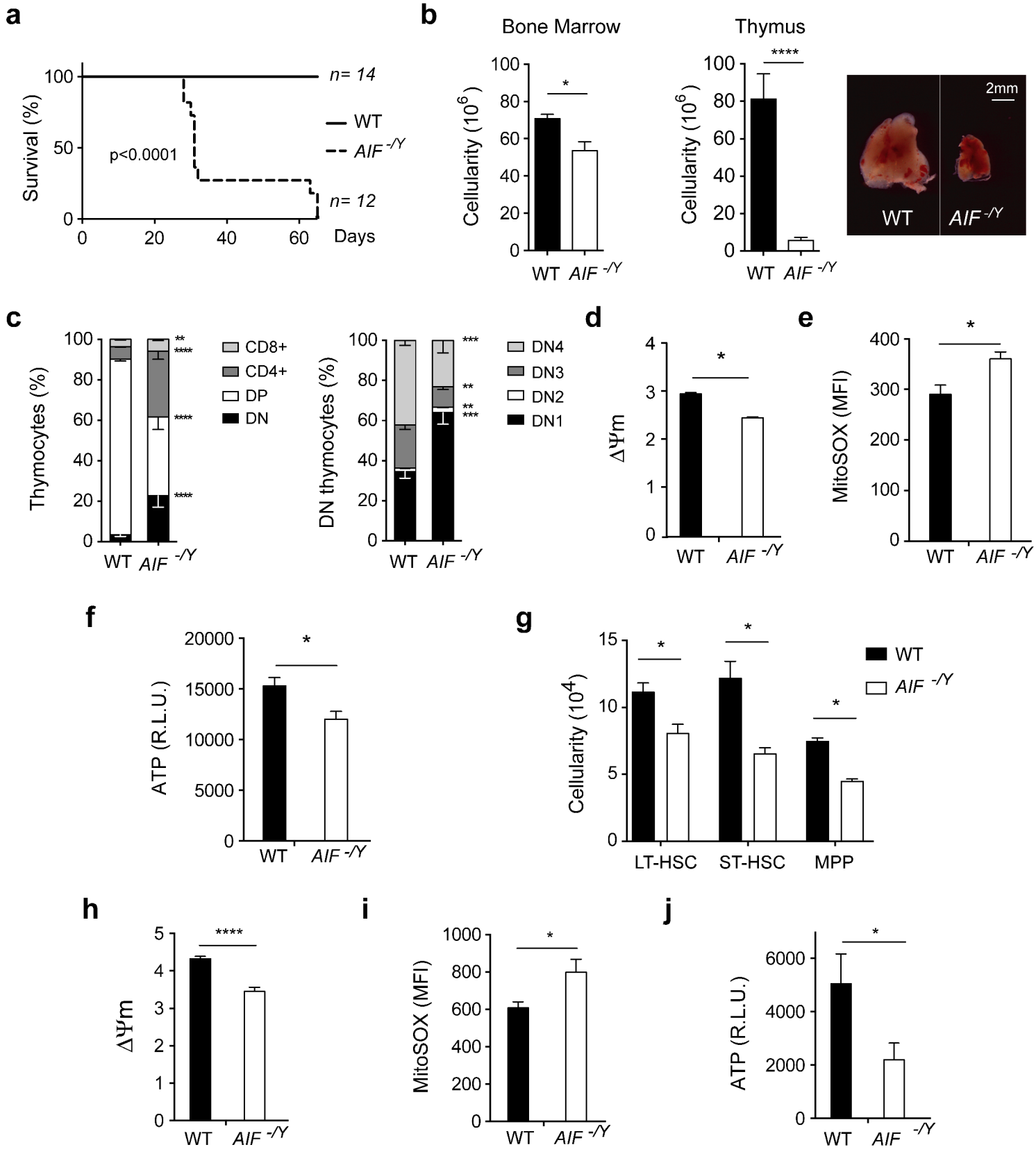

Supplementary Figure 3. AIF loss provoked hematopoietic defaults in adult mice. (**a**) Kaplan- Meier survival probability of WT and *AIF* $^{-/Y}$ tamoxifen-treated mice. (**b**) Cellularity assessed in BM and thymus from WT and *AIF* $^{-/Y}$ mice (n = 8 animals per group). Representative images of a thymus from control and *AIF* $^{-/Y}$ mice are shown. (**c**) Left, percentages of CD4-/CD8- (DN), CD4+/CD8+ (DP), CD4+, and CD8+ thymocytes in WT and *AIF* $^{-/Y}$ tamoxifen-treated mice (n = 12 animals per group). *Right*, fre quencies of DN1-DN4 thymocytes from WT and *AIF* $^{-/Y}$ tamoxifen-treated animals (n = 12 mice per group). (**d**) ΔΨm assessment performed in BM cells from WT and *AIF* $^{-/Y}$ tamoxifen-treated mice (n = 12 animals per group). (**e**) Mitochondrial ROS levels recor ded in BM cells obtained from WT and *AIF* $^{-/Y}$ tamoxifen-treated animals (n = 9 mice per group). (**f**) ATP levels recorded in BM cells obtained from WT and *AIF* $^{-/Y}$ tamoxifen-treated animals (n = 6 mice per group). (**g**) The number of LT-HSC, ST-HSC, and MPP assessed in WT and *AIF* $^{-/Y}$ mice (n = 7 animals per group). **(h)** ΔΨm assessment performed in thymocytes from WT and *AIF* $^{-/Y}$ ta moxifen-treated mice (n = 9 animals per group). (**i**) Mitochondrial ROS levels recorded in thymocytes obtained from WT and *AIF* $^{-/Y}$ tamoxifen-treated animals (n = 9 mice per group). (**j**) ATP levels recorded in thymocytes obtained from WT and *AIF* $^{-/Y}$ tamoxifen-treated animals (n = 6 mice per group). Statistical significance was calculated by Mann Whitney test in samples obtained from mi ce 28 days after the first tamoxifen injection. Bars represent mean ± SEM. *Aifm1* $^{fl/Y}$*;Rosa26-CreERT2*- tamoxifen-injected mice were used as control (WT) animals.

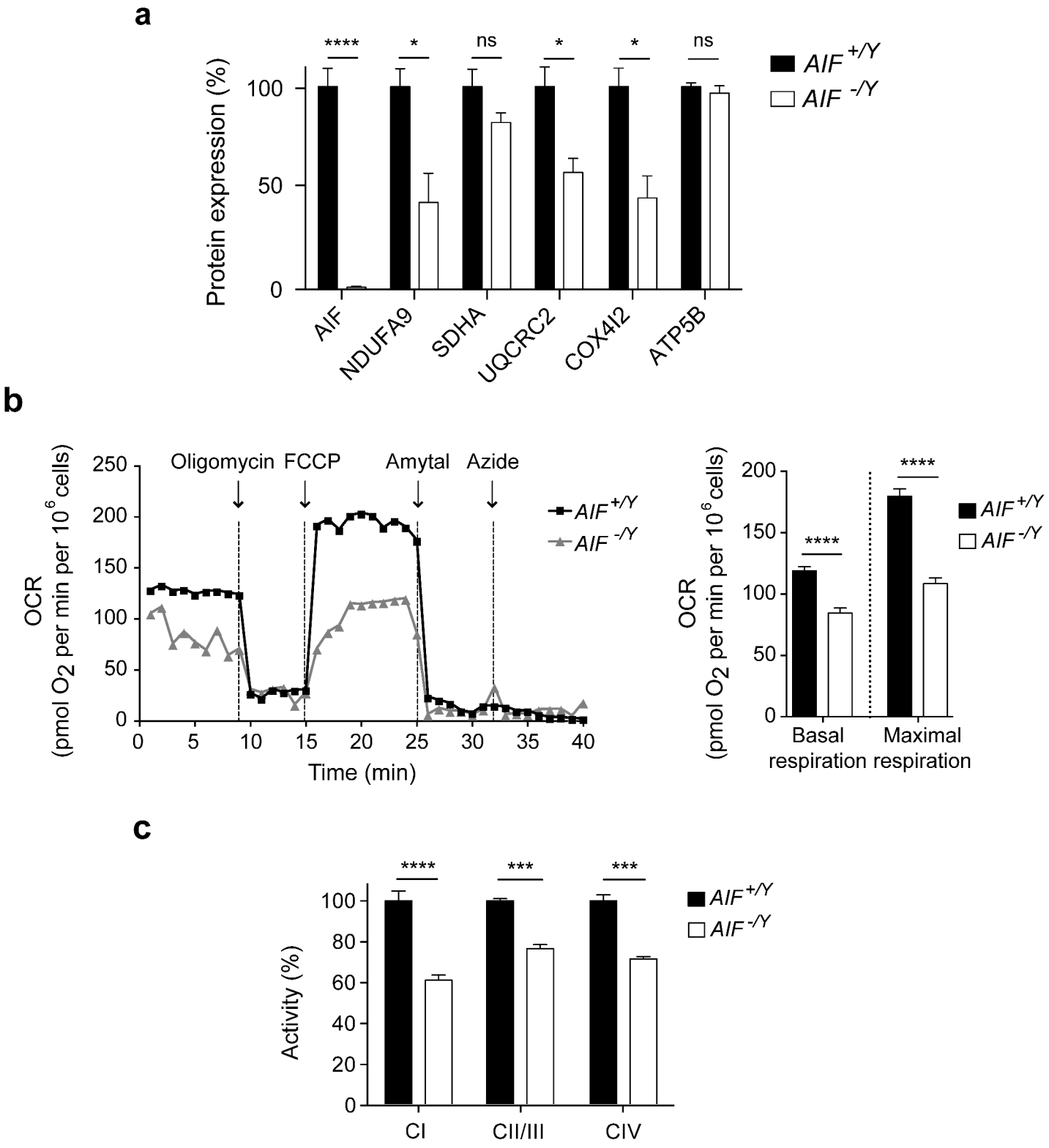

Supplementary Figure 4. AIF deficiency induced loss of ETC integrity and OXPHOS dysfunction. (**a**) AIF, NDUFA9, SDHA, UQCRC2, COX4I2, and ATP5B protein expression, verified by immunoblotting in **Figure 2a**, was quantified as indicated in the Materials and Methods section. Data are expressed as a percentage relative to the mean of the OD obtained in the *AIF* $^{+/Y}$ BM samples (100 %). (**b**) *Left*, Clark electrode OCR curve representing basal oxygen respiration (initial rates) of *AIF* $^{+/Y}$ or *AIF* $^{-/Y}$ BM cells and cell response to oligomycin, FCCP, amytal, and azide sequential addition. Arrows indicate the time of the addition of each substrate. *Right,* Basal and maximal oxygen consumption rates in BM cells from *AIF* $^{+/Y}$ or *AIF* $^{-/Y}$ animals (n = 5 independent experiments). (**c**) Complex I (Malate + Glutamate), II/III (Succinate), and IV (TMPD + Ascorbate)-driven OCR of permeabilized *AIF* $^{+/Y}$ or *AIF* $^{-/Y}$ BM cells measured by Seahorse. Data obtained in *AIF* $^{-/Y}$ cells are expressed as a percentage of the activity recorded in *AIF* $^{+/Y}$ cells (100 %) (n = 8 from 2 independent experiments). Statistical significance was calculated by *t*-student (**a**) or Mann Whitney (**b** and **c)** tests. Bars represent mean ± SEM.

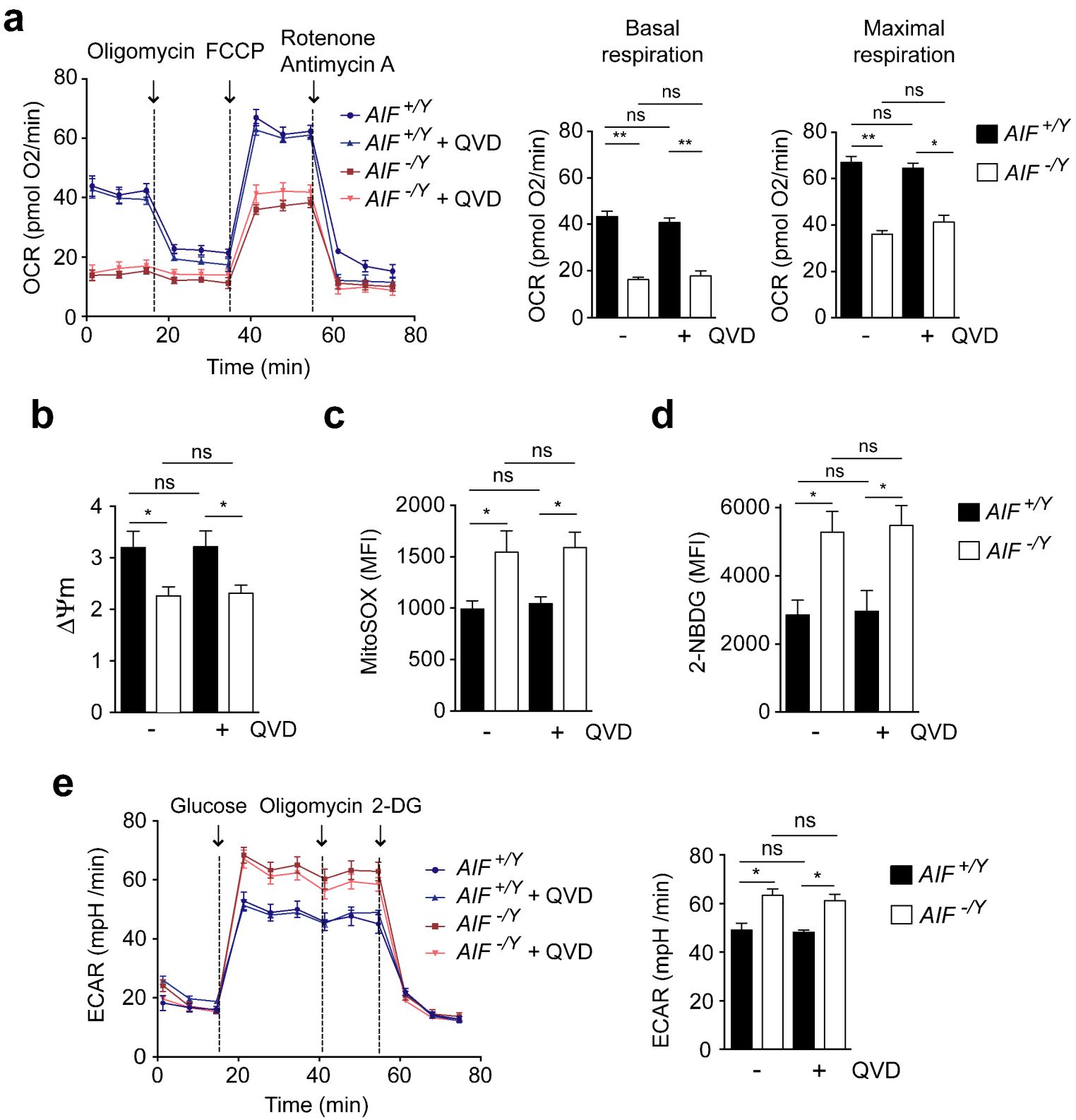

Supplementary Figure 5. The metabolic changes associated to AIF deficiency in BM cells are caspase-independent. (**a**) *Left*, Representative Seahorse OCR assessment of *AIF* $^{+/Y}$ and *AIF* $^{-/Y}$ BM cells pretreated or not during 30 min with the caspase inhibitor Q-VD-OPh (QVD, 1 µM) under basal conditions (initial rates) and in response to sequential treatment with Oligomycin, FCCP, and Rotenone/Antimycin A. Arrows indicate the time of the addition of each reagent. *Right*, Basal and ma ximal OCR of BM cells ± QVD expressed as a histogram (n = 3 independent experiments). (**b**) ΔΨm assessment performed in *AIF* $^{+/Y}$ and *AIF* $^{-/Y}$ BM cells ± QVD (n = 6 mice per group). (**c**) Mitochon drial ROS levels recorded in *AIF* $^{+/Y}$ and *AIF* $^{-/Y}$ BM cells ± QVD (n = 6 mice per group).(**d**) Glucose uptake measured by the assimilation of 2-NBDG in *AIF* $^{+/Y}$ and *AIF* $^{-/Y}$ BM cells ± QVD (n = 5 mice per group). (**e**) Representative ECAR of *AIF* $^{+/Y}$ and *AIF* $^{-/Y}$ BM cells ± QVD measured in response to sequential addition of Glucose, Oligomycin, and 2-deoxyglucose (2-DG). Arrows indicate the time of the addition of each reagent. *Right*, ECAR of BM cells ± QVD after Glucose treatment expressed as a histogram (n= 3 independent experiments). Statistical significance was calculated by Mann Whitney test. Bars represent mean ± SEM. All tests were performed in BM cells from 21-day-old animals.

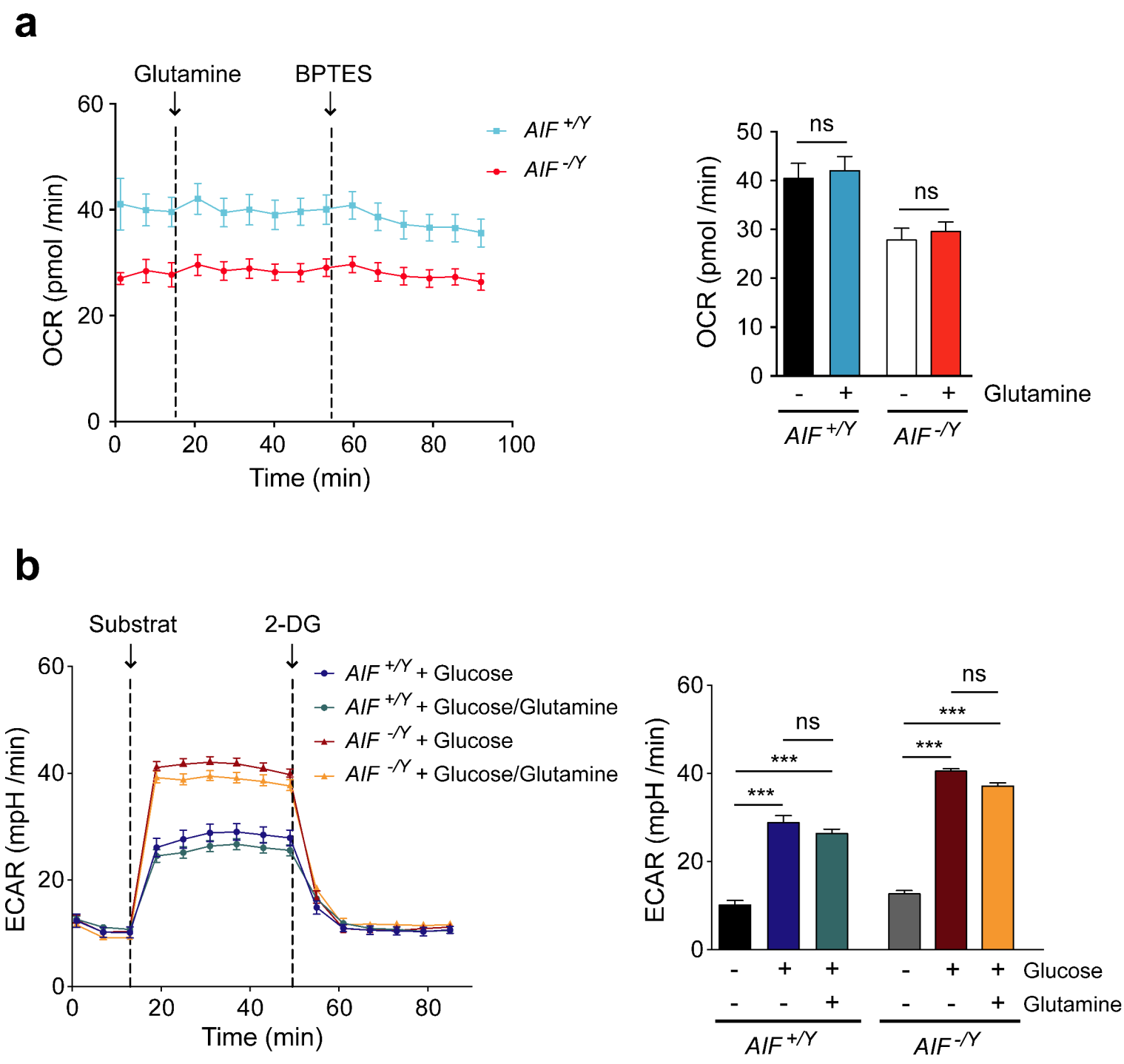

Supplementary Figure 6. *AIF*$^{-/Y}$ BM cells do not use glutaminolysis as a source of energy. (**a**) *Left,* Representative Seahorse OCR assessment of *AIF*$^{+/Y}$ and *AIF*$^{-/Y}$ BM cells from 21-day-old animals under basal conditions (initial rates) and in response to the sequential treatment with Glutamine and BPTES (a selective inhibitor of Glutaminase). Arrows indicate the time of the addition of each reagent. Note the absence of response to the treatments (OCR increase or inhibition). *Right*, OCR of *AIF*$^{+/Y}$ and *AIF*$^{-/Y}$ BM cells after Glutamine treatment expressed as a histogram (n = 3 independent experiments). (**b**) *Left*, Representative Seahorse ECAR assessment of *AIF*$^{+/Y}$ and *AIF*$^{-/Y}$ BM cells measured in response to sequential addition of Glucose or Glucose+Glutamine (Substrat) and 2-deoxyglucose (2-DG). Arrows indicate the time of the addition of each reagent. Note the absence of response to Glutamine addition and the total inhibition by 2-DG. *Right*, ECAR *AIF*$^{+/Y}$ and *AIF*$^{-/Y}$ BM cells after the indicated treatment expressed as a histogram (n = 3 independent experiments). Statistical significance was calculated by Mann Whitney test. Bars represent mean ± SEM.

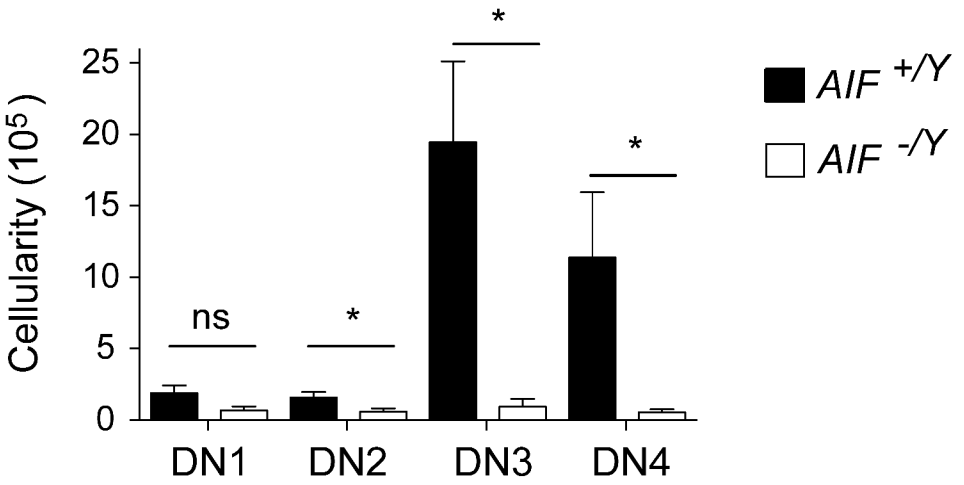

Supplementary Figure 7. AIF loss induced a significant reduction in DN2, DN3, and DN4 thymocyte subsets . After a flow cytometry CD4, CD8, CD25, and CD44 labelling, the number of DN1-DN4 thymocytes in 7-day-old *AIF* $^{+/Y}$ and *AIF* $^{-/Y}$ animals was counted and expressed as a histogram (n = 5 mice per group). Statistical significance was calculated by Mann Whitney test. Bars represent mean ± SEM.

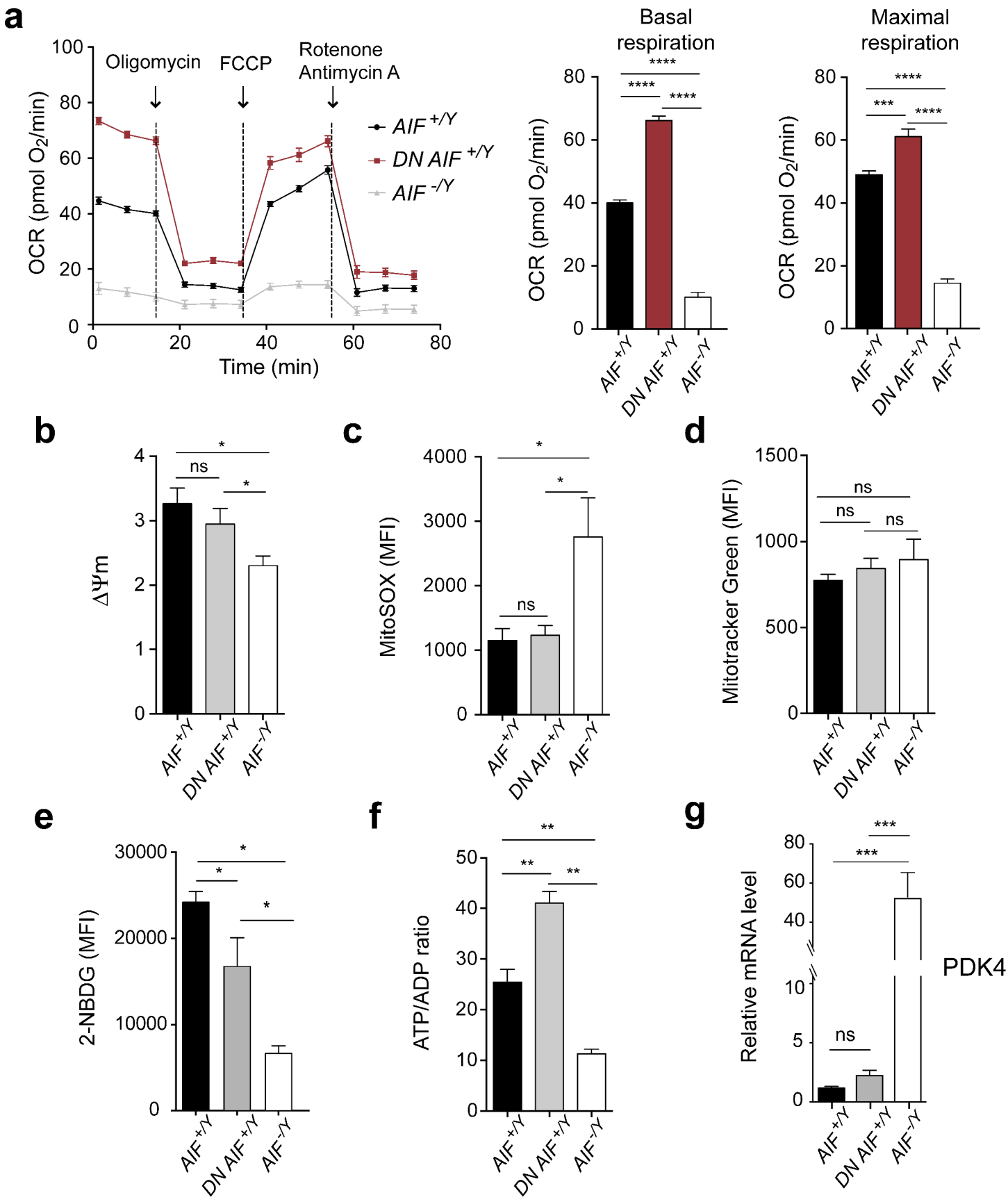

Supplementary Figure 8. The metabolic reprogramming induced by AIF loss was confirmed by confronting the *AIF +/Y*, DN *AIF +/Y*, and *AIF -/Y* thymocyte compartments. (**a**) *Left*, Representative Seahorse OCR assessment of *AIF +/Y*, DN *AIF +/Y*, and *AIF -/Y* thymocytes under basal conditions and in response to sequential treatment with Oligo mycin, FCCP, and Rotenone/Antimycin A. Arrows indicate the time of the addition of each reagent. *Right*, Basal and ma ximal OCR of thymocytes expressed as a histogram (n = 3 independent experiments). (**b**) ΔΨm assessment performed in *AIF +/Y*, DN *AIF +/Y*, and *AIF -/Y* thymocytes (n = 6 mice per group).(**c**) Mitochondrial ROS levels recorded in *AIF +/Y*, DN *AIF +/Y*, and *AIF -/Y* thymocytes (n = 8 mice per group). (**d**) Mitochondrial mass of *AIF +/Y*, DN *AIF +/Y*, and *AIF -/Y* thy mocytes assessed by Mitotracker Green labeling (n = 8 mice per group). (**e**) Glucose uptake measured by the assimilati on of 2-NBDG in *AIF +/Y*, DN *AIF +/Y*, and *AIF -/Y* thymocytes (n = 5 mice per group).(**f**) ATP levels recorded in *AIF +/Y*, DN *AIF +/Y*, and *AIF -/Y* thymocytes (n = 5 mice per group). (**g**) PDK4 mRNA levels determined by qPCR in *AIF +/Y*, DN *AIF +/Y*, and *AIF -/Y* thymocytes (n = 8 mice per group). The 18S mRNA expression was used to normalize the data. Statistical significance was calculated by Mann Whitney test. Bars represent mean ± SEM. All tests were performed in 21-day-old animals.

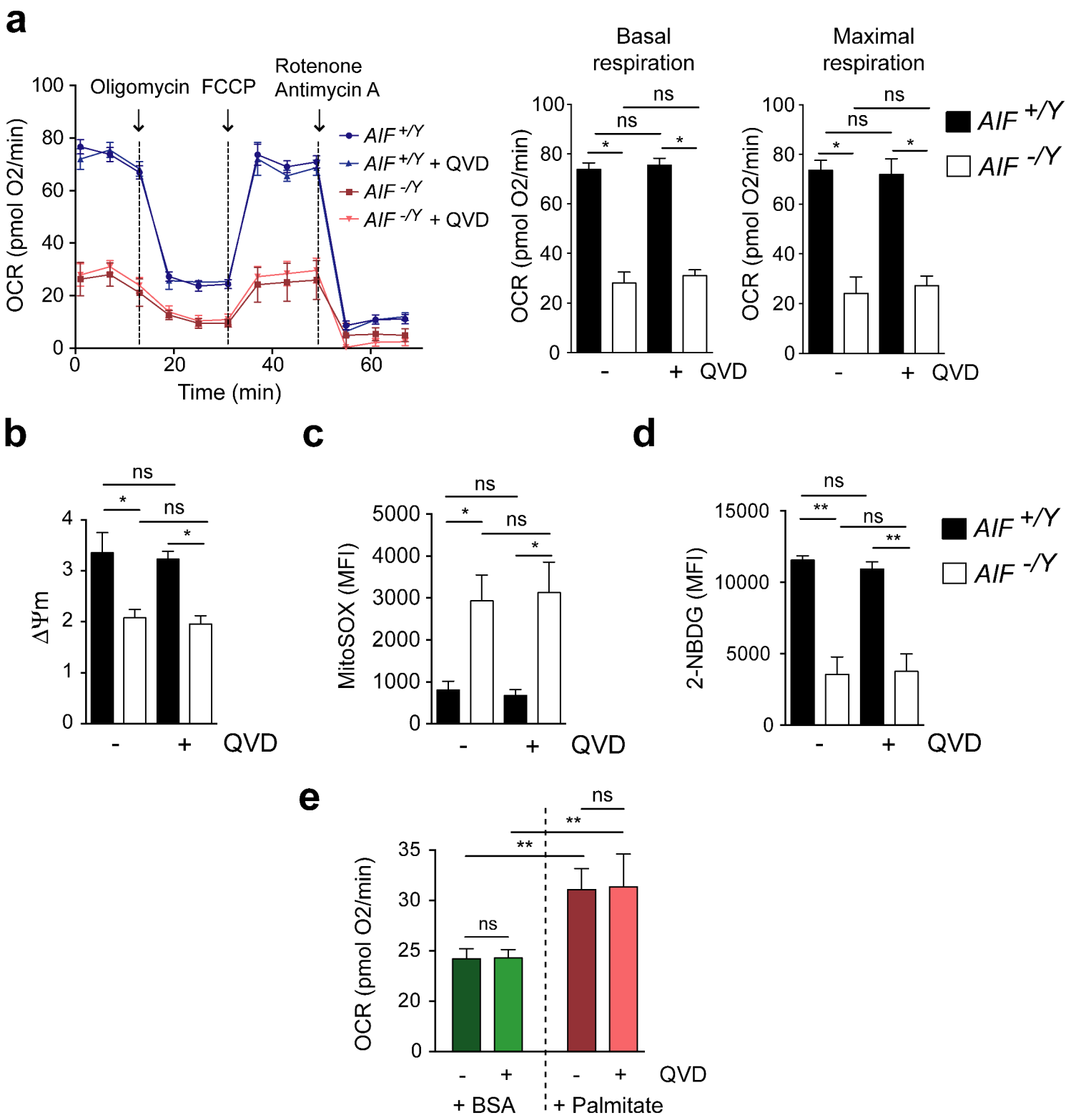

Supplementary Figure 9. The metabolic changes associated to AIF deficiency in thymocytes are caspase-independent. (**a**) *Left*, Representative Seahorse OCR assessment of *AIF* $^{+/Y}$ and *AIF* $^{-/Y}$ thymocytes pretreated or not during 30 min with the caspase inhibitor Q-VD-OPh (QVD, 1 µM) under basal conditions (initial rates) and in response to sequential treatment with Oligomycin, FCCP, and Rotenone/Antimycin A. Arrows indicate the time of the addition of each reagent. *Right*, Basal and ma ximal OCR of thymocytes ± QVD expressed as a histogram (n = 3 independent experiments). (**b**) ΔΨm assessment performed in *AIF* $^{+/Y}$ and *AIF* $^{-/Y}$ thymocytes ± QVD (n = 6 mice per group). (**c**) Mitochon drial ROS levels recorded in *AIF* $^{+/Y}$ and *AIF* $^{-/Y}$ thymocytes ± QVD (n = 4 mice per group).(**d**) Glucose uptake measured by the assimilation of 2-NBDG in *AIF* $^{+/Y}$ and *AIF* $^{-/Y}$ thymocytes ± QVD (n = 5 mice per group). (**e**) Representative Seahorse OCR assessment in thymocytes from *AIF* $^{-/Y}$ 21-day-old ani mals pretreated or not with QVD. After measurement of basal OCR, BSA control or Palmitate-BSA FAO Substrate (17 µM) were injected and maximar OCR was measured and expressed as a histo gram (n= 3 independent experiments). Statistical significance was calculated by Mann Whitney test. Bars represent mean ± SEM. All tests were performed in thymocytes from 21-day-old animals.

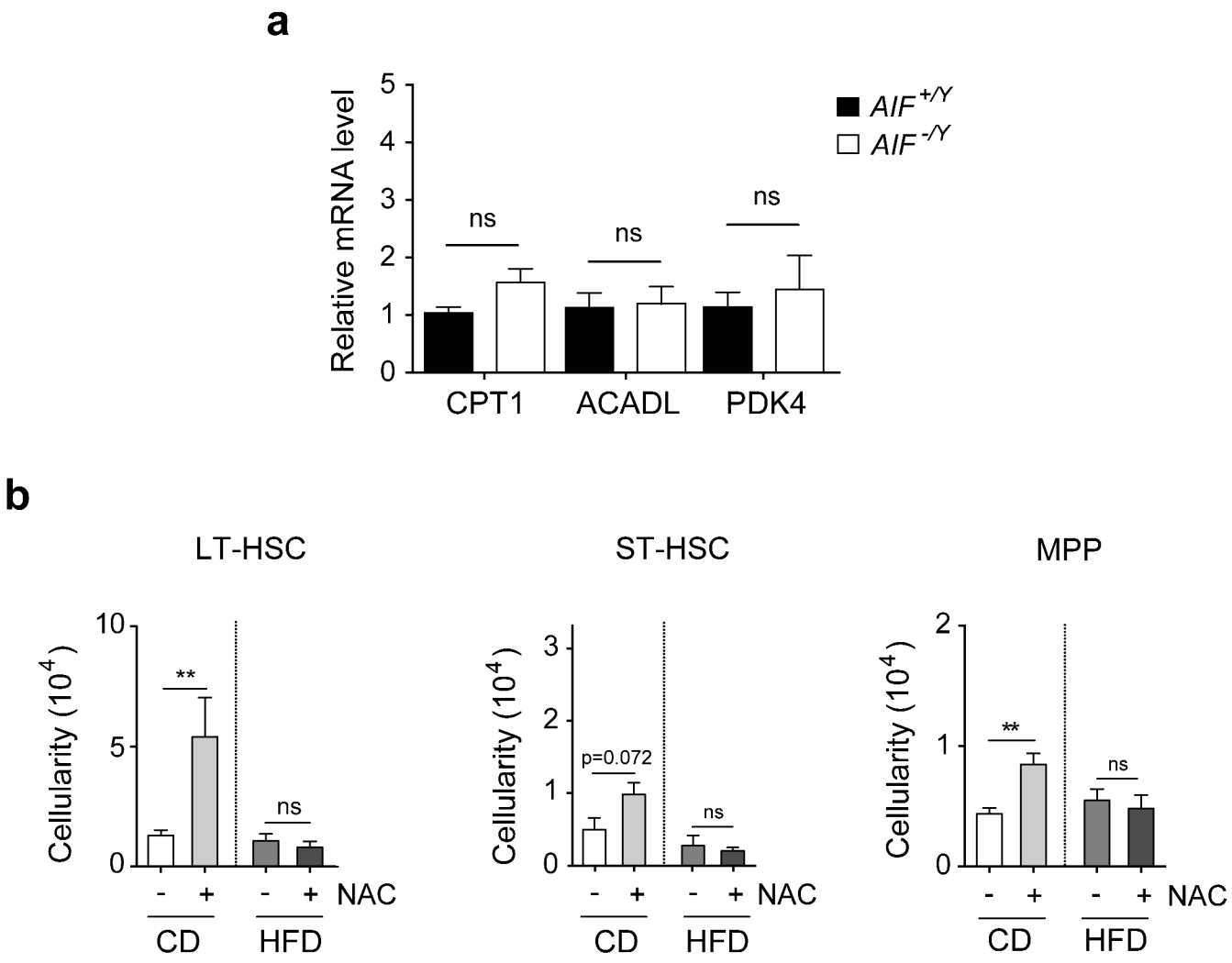

Supplementary Figure 10. *AIF*$^{-/Y}$ HSC and MPP were unable to shift towards a fatty acid metabo lism. (**a**) CPT1, ACADL, and PDK4 mRNA levels determined by quantitative RT-PCR in *AIF*$^{+/Y}$ and *AIF*$^{-/Y}$ BM cells from 21-day-old animals (n = 4 mice per group). The 18S mRNA expression was u sed to normalize the data. (**b**) Dams were fed a standard control diet (CD) or high-fat diet (HFD) and were supplied or not with NAC in drinking water; the number of LT-HSC, ST-HSC, and MPP cells from *AIF*$^{-/Y}$ 21-day-old newborns was counted and expressed as a histogram (n = 8 mice per group). Statistical significance was calculated by Mann Whitney test. Bars represent mean ± SEM.